Rapid method for preliminary identification of subthreshold strongly lensed counterparts to superthreshold gravitational-wave events

Srashti Goyal,[1,6] Shasvath J. Kapadia,[2] Jean-René Cudell,[3] Alvin K. Y. Li,[4] and Juno C. L. Chan[5]

[1]*International Centre for Theoretical Science, Tata Institute of Fundamental Research, Bangalore 560089, India*

[2]*Inter-University Centre for Astronomy and Astrophysics, Post Bag 4, Ganeshkhind, Pune 411007, India*

[3]*STAR Institute, Université de Liège, 4000 Liège, Belgium*

[4]*LIGO Laboratory, California Institute of Technology, Pasadena, California 91125, USA*

[5]*Niels Bohr International Academy, Niels Bohr Institute, Blegdamsvej 17, 2100 Copenhagen, Denmark*

[6]*Max Planck Institute for Gravitational Physics (Albert Einstein Institute), Am Mühlenberg 1, D-14476 Potsdam-Golm, Germany*

(Received 16 June 2023; accepted 20 December 2023; published 29 January 2024)

Gravitational waves (GWs) from stellar-mass compact binary coalescences (CBCs) are expected to be strongly lensed when encountering large agglomerations of matter, such as galaxies or clusters. Searches for strongly lensed GWs have been conducted using data from the first three observing runs of the LIGO-Virgo GW detector network. Although no confirmed detections have been reported, interesting candidate lensed pairs have been identified. In this work, we delineate a preliminary analysis that rapidly identifies pairs to be further analyzed by more sophisticated Bayesian parameter estimation (PE) methods. The analysis relies on the Gaussian/Fisher approximation to the likelihood and compares the corresponding approximate posteriors on the chirp masses of the candidate pair. It additionally cross-correlates the rapidly produced localization sky areas (constructed by Bayestar sky-localization software). The analysis was used to identify pairs involving counterparts from targeted subthreshold searches to confidently detected superthreshold CBC events. The most significant candidate "super-sub" pair deemed by this analysis was subsequently found, by more sophisticated and detailed joint-PE analyses, to be among the more significant candidate pairs, but not sufficiently significant to suggest the observation of a lensed event [J. Janquart *et al.*, Follow-up analyses to the O3 LIGO-Virgo-KAGRA lensing searches, Mon. Not. R. Astron. Soc. **526**, 3 (2023)].

DOI: 10.1103/PhysRevD.109.023028

I. INTRODUCTION

The LIGO-Virgo-KAGRA [1–3] network of ground-based, interferometric, gravitational wave (GW) detectors has completed three observing runs: O1, O2, and O3. These runs have provided ∼100 detections of compact binary coalescence (CBC) events [4–9]. The majority of these correspond to binary black hole (BBH) mergers, although binary neutron star (BNS) [10,11] and neutron star black hole (NSBH) [12] binary mergers have also been observed.

These detections have enabled many novel probes of various aspects of astrophysics, cosmology, and fundamental physics, including constraints on the populations of stellar-mass compact binaries that merge within Hubble time [13], distance-ladder-independent measurements of the Hubble constant [14], unique tests of general relativity in the strong-field regime [15], and the nature of matter at extreme densities via constraints on the neutron star equation of state [16]. Nevertheless, several discoveries involving GWs still remain to be made. Among them is the anticipated observation of gravitationally lensed GWs. Propagating GWs, like light, will have their paths deviated if they encounter matter inhomogeneities [17–20]. In particular, when GWs from stellar mass CBCs, detectable by LIGO-Virgo, encounter galaxies or clusters, they will be strongly lensed, resulting in the possible production of multiple temporally resolvable images [21–24]. These images are (de)magnified copies of the source separated by time delays that span minutes to weeks for galaxy lenses and up to a few years for galaxy cluster lenses. Thus, they will have identical phase evolution, although their amplitudes will generally differ by a multiplicative constant factor (see, e.g., [25]). In addition, a constant phase difference of either 0, $\pi/2$, or π, called the Morse phase, will be incurred between the images, depending on the image type (type I, II, or III [26,27]).

Several techniques have been devised to search for such strongly lensed pairs of GW events, most of which rely on the identical phase evolution of the images, the superposed GW localization sky areas of the images [28], and the Morse phase. These include two low-latency techniques. One is a machine learning (ML)-based method that compares time-frequency maps and localization sky areas of individual

events in a candidate lensed pair [29]. The other is a posterior overlap (PO) method that compares the existing Bayesian posterior distribution of the (intrinsic and sky location) parameters of individual events acquired from large-scale Bayesian parameter estimation (PE) exercises [25]. Other more comprehensive though computationally expensive methods involve sampling a joint likelihood, constructed from the GW likelihoods of the individual events in the candidate lensed pair [30–33]. Each of these methods has been employed to search for lensed pairs involving super-threshold/confidently detected GW events from O1, O2, and O3 [4,34,35]. No candidate pair was deemed sufficiently significant to claim detection of GW lensing [36–38].

It has been suggested in the literature that the rate of lensed events—where one event in a lensed pair is a superthreshold GW event, while the other is a subthreshold event whose reduced significance could be due to one (or more) of several reasons, including demagnification—is larger by a factor of few than the rate of lensed pairs where both GW events are superthreshold [39]. It is therefore worthwhile to search for such "super-sub" lensed pairs. A lensed GW counterpart can be missed by the usual matched-filter searches due to its low signal-to-noise ratio (SNR) as a result of lensing demagnification or reduced sensitivity of the detector for certain parameters of the source. Hence, a separate matched-filter search is done to find the possible subthreshold lensed counterparts for each of the targeted superthreshold events [40,41]. This is done by utilizing the posteriors of intrinsic parameters of the superthreshold events to construct a reduced template bank that enables a deeper search for subthreshold events by reducing the background noise. The candidate super-sub pairs have been found through these searches during O2 [41,42] and O3 [38]. However, till now, no confident detection has been made.

While all the superthreshold candidates [events having a search false-alarm rate (FAR) $<2/\text{day}$ and $p_{\text{astro}} > 0.5$ as per the GW transient catalogs, GWTC-2.1 [43] and GWTC-3 [4]] have PE posteriors readily available,[1] the subthreshold candidates generally do not. This is in part because there is not sufficient evidence to suggest that they are of astrophysical origin and therefore worthy of PE follow-up.

Moreover, acquiring PE samples for all the subthreshold candidates is computationally taxing, which makes most of the existing lensing-identification methods mentioned above too computationally expensive and time consuming to be feasibly used. This is true even for the low-latency approaches. PO requires PE posteriors on the intrinsic parameters of both events in the lensed pair candidate to be analyzed [25]. On the other hand, the ML-based method needs extensive training and testing involving subthreshold events, which has yet to be completed [29]. To mitigate the increase in candidate pairs by including subthreshold events, we introduce another method that rapidly constructs interpretable, albeit approximate, statistics to rank the candidate lensing counterparts to the superthreshold events that are found by the targeted subthreshold searches. The method then provides a *preliminary* identification of super-sub lensed candidate pairs.

Our method is akin to PO, although the data products used can be generated rapidly without taxing computational resources. In particular, the GW likelihood is approximated as a Gaussian using a Fisher analysis [46]. This enables a rapid, though approximate, construction of posterior distributions on the chirp masses of the super-/subthreshold events. For each super-sub candidate pair, the chirp-mass posteriors of the events in the pair are quantitatively compared using the Bhattacharyya distance [47]. Another coefficient is produced by cross-correlating the Bayestar sky maps [48], generated in low latency, of each of the events in the pair. A third coefficient, exploiting the expected time delay distribution of detected strongly lensed events, is also constructed. The coefficient values are then sorted in descending order to identify any super-sub candidate pair with large values across all three coefficients.

All super-sub candidate pairs were found to be insignificant by one or more of these statistics, with the notable exception of one solitary outlier, GW191230_180458–LGW200104_180425, which we call simply GW191230-LGW200104 from now on. This pair lies in the top-fifth percentile of all super-sub pairs across all three statistics. The event pair was reanalyzed by PO and more sophisticated joint-PE methods [31,32] and found to be among the more significant candidate pairs, though not sufficiently significant to claim observation of lensing. We point the reader to [49] for more detailed analyses of this event pair.

The rest of the paper is organized as follows: Section II describes the construction of the approximate statistics. Section III describes the results, including the performance of the approximate statistic on synthetic lensed and unlensed events as compared to PO, as well as the output of the method applied to the super-sub pairs. Section IV summarizes the paper and discusses the scope for future improvements.

II. METHODS

Given a pair of CBC events, we wish to determine whether they have a common provenance (lensed), or whether they are unrelated (unlensed). In the geometrical optics limit, each strongly lensed copy of the GW strain gets an overall magnification, time delay, and a (Morse) phase shift, although the phase evolution remains unaffected. In addition, the angular separation of the images [$\mathcal{O}(1'')$ or smaller] is orders of magnitude smaller than what can be resolved with GW detectors [which provide sky areas of $\mathcal{O}(10)$ sq. deg or larger].

[1]The posterior samples are found in the data releases [44] and [45].

Hence, apart from luminosity distance, time of arrival, and coalescence phase, the Bayesian inference of intrinsic and extrinsic parameters should yield posterior distributions that overlap well. The PO statistic exploits this fact to distinguish between the lensed and unlensed candidate pairs. However, its reliance on the availability of PE posteriors makes it difficult to employ to identify subthreshold image counterparts to superthreshold GW events. This is because PE posteriors are computationally expensive and time-consuming to produce and are thus usually unavailable for subthreshold events.

On the other hand, the matched-filter-based search pipelines give point estimates of the intrinsic parameters and the GW network's signal-to-noise ratio (SNR). Furthermore, the chirp mass of a CBC is expected to be the best measured among all intrinsic parameters, certainly for those events whose in-band signal is dominated by the inspiral. We use this to construct a statistic, $\mathcal{B}^{\rm masses}$, that estimates a "distance" separating the chirp-mass posteriors evaluated using a Fisher analysis.

Additionally, we use the Bayestar [48] sky localization software to rapidly reconstruct the localization sky maps. We then cross-correlate them to evaluate another statistic, $\mathcal{B}^{\rm sky}$, that measures the degree of overlap between these sky maps.

And finally, we use the $\mathcal{R}_{\rm gal}$ [25,50] statistic to assess if the time delay of the candidate is more consistent with the distribution of temporal separations of randomly distributed events within the observation time, or the distribution of simulated image time delays constructed from an assumed distribution of galaxy lenses and sources.

A. Bayestar sky maps

"Bayestar" is sky localization software that can produce sky maps in seconds by exploiting the fact that the intrinsic and extrinsic parameters of a CBC are semi-uncorrelated. It pins the intrinsic parameters to their matched-filter search point estimates and rapidly marginalizes out the remaining nuisance parameters using Gaussian quadrature methods, to provide a posterior on the right ascension (α) and declination (δ) of the source [48].

Following [29], we project the Bayestar sky maps to a Cartesian grid ($N_\alpha \times N_\delta$) of the sky coordinates (α, δ). For each of the two images d_1 and d_2, we then have the probability of an event happening in bin (α_i, δ_j) as $P^1_{i,j}$ and $P^2_{i,j}$. With these matrices, we evaluate the following statistic, which is motivated by the PO statistic [25]:

$$\mathcal{B}^{\rm sky} = \int \frac{P(\alpha,\delta|d_1)P(\alpha,\delta|d_2)}{P(\alpha,\delta)} \sin\delta d\alpha d\delta \approx \frac{8\pi^3}{N_\alpha \times N_\delta} \Sigma_i \Sigma_j P^1_{i,j} P^2_{i,j}. \quad (1)$$

If the two images do not overlap at all, then $\mathcal{B}^{\rm sky} = 0$. Numerically, to evaluate this statistic, we used $N_\alpha = 800$ and $N_\delta = 400$, which we found to be accurate enough for the typical sky resolution of the GW events by current-generation detectors.

B. Chirp masses

The search pipelines report the detector frame matched-filtered chirp mass, $\mathcal{M}^{\rm det}_c$, and the SNR for the triggers based on the best match template at each detector. Following [51], we construct a likelihood on the chirp mass for each image, $p(d_i|\mathcal{M}^{\rm det}_c)$, as a Gaussian with the mean as the average of matched-filtered chirp masses over detectors and standard deviation as

$$\Delta(\log \mathcal{M}^{\rm det}_c) = 0.08(\rho_{\rm thresh})/\rho, \quad (2)$$

where ρ is the network SNR for the triggers and $\rho_{\rm thresh} = 8$. The Bhattacharyya coefficient in chirp mass ($\mathcal{B}^{\rm masses}$) is defined as

$$\mathcal{B}^{\rm masses} = \int \sqrt{P(d_1|\mathcal{M}^{\rm det}_c)P(d_2|\mathcal{M}^{\rm det}_c)}\, d\mathcal{M}^{\rm det}_c, \quad (3)$$

which is our second statistic for rapid lensing identification. Note that unlike the PO statistic [Eq. (5)], the Bhattacharyya coefficient is normalized, ranging from 0 to 1. The integral in Eq. (3) is simplified for the Gaussian probability distributions and can be written in terms of means and standard deviations of the two Gaussians.

In Gaussian noise, the matched-filter SNR is an optimal statistic. However, non-Gaussianities in real noise can produce spuriously large SNRs. Furthermore, even in Gaussian noise, noise fluctuations and discreteness of the template bank could result in signals being recovered by templates whose parameters are significantly biased with respect to the true source parameters.

We compare in Fig. 1 the estimates of chirp mass from PE with the matched-filter estimates for GWTC-3 events. The PE estimates are taken from GWOSC [52], whereas the matched-filter estimates are taken from GraceDB, as reported by the search pipelines [53–55]. About 13 out of 81 events have a $\mathcal{M}^{\rm det}_c$ from the matched-filter values that is significantly different (mostly overestimated) with respect to the PE estimates. This is seen in the figure as points sufficiently deviated from the diagonal such that neither the vertical nor the horizontal error bar intersects the diagonal. Most of these events are in the chirp mass range 40–$60M_\odot$. We do not find any correlation with the SNR for these biases. In addition to the chirp mass, the matched-filter searches also output the best-fit template's mass ratio and spins. This information can in principle be considered for lensing identification; however, we leave this for future work.

The lower chirp mass binaries are less biased than the high ones due to their longer inspiral in the frequency band of LIGO-Virgo detectors. This is clearly a caveat but is

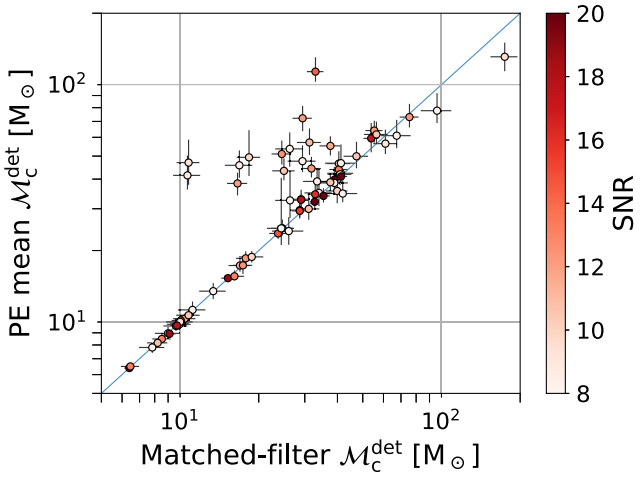

FIG. 1. Chirp mass estimates from PE and matched-filter-based searches for the GWTC-3 events. About 10%–15% of events are significantly biased—the mean value of the detector-frame chirp mass lies outside the 90% confidence range of the corresponding PE posteriors (vertical error bars) and matched-filter chirp masses (horizontal error bars) coming from Eq. (2). If these error bars cross the diagonal, then the corresponding events should not be considered as significantly biased. The lower chirp mass binaries are less biased than the high ones due to their longer inspiral in the frequency band of LIGO-Virgo detectors.

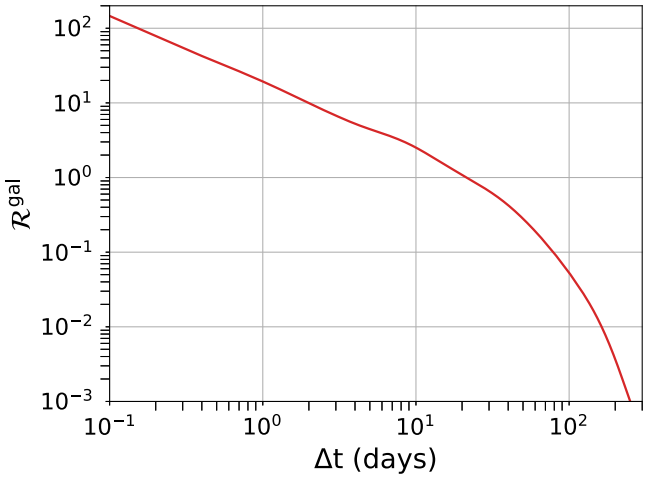

FIG. 2. $\mathcal{R}^{gal}$ statistic as a function of the time delay between the events, assuming the O3 observation time. This is a model-dependent statistic—the galaxy lens is assumed to be a singular isothermal ellipsoid, and the lens parameters are fit to the SDSS catalog. Lens redshifts are also assumed to follow the SDSS catalog, while source masses assume a power-law + peak model.

partially mitigated by the fact that the Bhattacharyya coefficient is not used in isolation, but in conjunction with other statistics in this section which are not susceptible to template biases.

C. Time-delay distributions

The time of arrival of GW signals is measured at $\mathcal{O}(\mathrm{ms})$ precision by matched-filter searches. It is therefore worthwhile to construct a statistic that uses arrival times as a means to discriminate between lensed and unlensed events. To that end, an $\mathcal{R}^{gal}$ statistic is constructed.

The distribution of time delays for unlensed pairs of GW signals $P(\Delta t|H_U)$ can be estimated by assuming the arrival times to follow a Poisson process [see Eq. (31) in [32]]. Conversely, the distribution of time delays for detectable lensed pairs depends on the distribution of lens parameters, source parameters, and the relative separations between the Earth, the lenses, and the sources.

For galaxy-scale lenses, the time delays could vary from several minutes to several weeks. For cluster-scale lenses, the time delays could even span months or years. Assuming an appropriate model for the distribution of galaxy-lens parameters, as well as the redshift distributions of lenses and sources, we can construct a distribution of time delays $P(\Delta t|H_L)$ [50] pertaining to detectable strongly lensed BBHs.

To construct this distribution, we simulate the lensed BBH populations by following the prescription which is mentioned in the appendix of [25]. In particular, the BBH mergers are distributed over redshift following Oguri *et al.* [56]. The mass spectrum of BBHs is assumed to be the power-law + peak model [13]. We assume the galaxy lens profile to be the singular isothermal ellipsoid (SIE) with which the lens equation is solved. The parameters, including redshifts, of the lens, are assumed to follow the SDSS catalog [57]. We set the detectability criteria[2] to be network SNR > 8.

The $\mathcal{R}^{gal}$ statistic is constructed from time-delay distributions of lensed and unlensed events as [25]

$$\mathcal{R}^{gal} = \frac{P(\Delta t_0|H_L)}{P(\Delta t_0|H_U)}, \tag{4}$$

where Δt_0 is the measured time delay between a given pair of signals. Figure 2 shows the $\mathcal{R}^{gal}$ statistic as a function of the time delay between the events, assuming the observation time of the full O3 run. The $\mathcal{R}^{gal}$ statistic favors small time delays and falls off rapidly with increasing time delays. Though this is a model-dependent statistic and valid only for galaxy lenses, it improves our capability of identifying lensed events from unlensed ones [25].

III. RESULTS

A. Assessment of the method with simulations

To assess the performance of our method, we first apply it to simulated lensed and unlensed events. These are injected in Gaussian noise, generated using the

[2]The subthreshold events in O3 have SNR > 7 (see Fig. 4); however, the time-delay distributions do not change noticeably with this choice.

zero-detuned high-power PSDs of Advanced LIGO and Advanced Virgo at their design sensitivities [58,59], as implemented in PYCBC [53,60]. We compare the performance of our method with the PO statistic, using the injection set given in [25] which consists of roughly 300 lensed pairs and 5×10^5 unlensed pairs. The PO statistic is given by the following integral:

$$\mathcal{B}^{\text{overlap}} = \int \frac{p(\vec{\theta}|d_1)p(\vec{\theta}|d_2)}{p(\vec{\theta})} d\vec{\theta}, \tag{5}$$

which in practice is evaluated by performing a Gaussian kernel density estimation on the posterior samples from the parameter-estimation runs of the individual events. This integral can be evaluated over all the parameters of the binary except the luminosity distance, coalescence phase, and coalescence time, as they would be biased due to lensing.

To calculate B^{masses}, we assume the likelihood in $\mathcal{M}_c^{\text{det}}$ to be Gaussian with the mean as the maximum-likelihood estimates from the PE runs (already performed over the mentioned injection set for the results of [25]) and use the SNR of the injection to calculate the standard deviation [see Eq. (2)]. We compare the performance of B^{masses} to the PO statistic $\mathcal{B}^{\text{overlap}}$ evaluated using the posteriors in component mass, setting $\vec{\theta} = \{m_1, m_2\}$ in Eq. (5). The maximum-likelihood estimates of the masses are a proxy for the matched-filter search estimates—a proxy that is expected to be a good approximation for Gaussian noise. For a templated search involving real noise, apart from the non-Gaussian nature of the latter, we would have an additional source of error in chirp mass estimation incurred due to template-bank discreteness.

To construct B^{sky}, we generate the Bayestar sky maps using the same injection parameters and noise properties as used in the PE runs mentioned above, and fixing the intrinsic parameters to their true values. We compare B^{sky} to the PO statistic $\mathcal{B}^{\text{overlap}}$ evaluated using the PE posteriors in the sky location, setting $\vec{\theta} = \{\alpha, \delta\}$ in Eq. (5).

We plot the receiver operating characteristics (ROCs) graphs in Fig. 3 for each statistic. The ROCs display the efficiency (i.e., the fraction of lensed events truly identified as lensed) at a given false positive probability (FPP, the fraction of unlensed events falsely identified as lensed).

An ideal classifier would have an efficiency of 1 for all FPPs. However, during lensing identification, false positives can arise due to chance overlaps of the posteriors of unrelated events. Hence, as we increase the threshold of a statistic to identify a pair as lensed, the number of false positives reduces, but at the cost of reducing the efficiency. As seen in the figure, both the mass-based and sky-map-based statistics produce reduced efficiencies relative to the PO method but are still better than a random classifier.

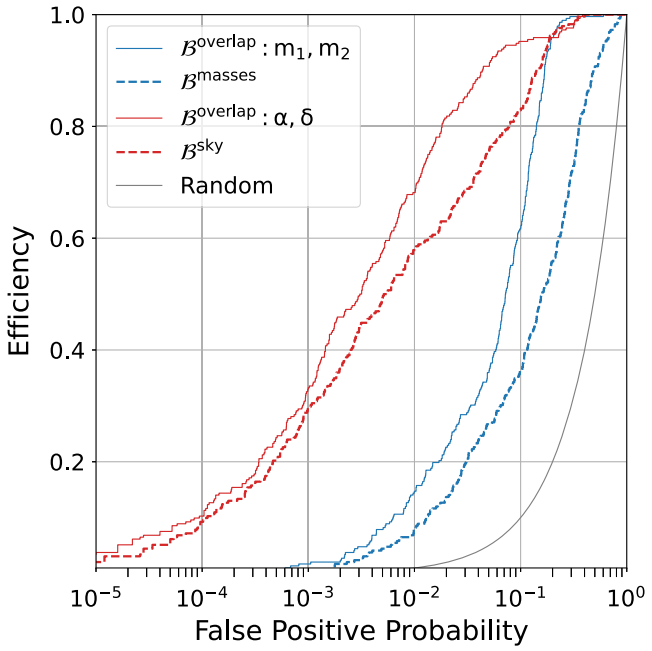

FIG. 3. Comparison of the rapid identification statistics against the PE-based PO method. There is only a partial loss in efficiency using these statistics relative to PO, and they all perform better than a random classifier that classifies a given pair as lensed or unlensed with probability 0.5, resulting in its efficiency being equal to the false positive probability (gray) curve.

B. O3 targeted subthreshold search triggers

In the case of strongly-lensed gravitational waves, a subthreshold event with the same intrinsic parameters as the superthreshold event is expected. We consider the GSTLAL-based TargetEd Sub-threshold Lensing seArch (TESLA) method [61] to search for subthreshold lensing counterparts. This is done using the posterior samples from the targeted superthreshold event to reduce the background noise. Since the lensed counterpart can be demagnified and obscured by noise, making it difficult to detect, it is necessary to minimize the impact of background noise. By reducing the amplitude and thus the optimal SNR, we generate these signals and inject them into actual data, which is analyzed using TESLA with a general template bank used in O3. We retain the templates that detect these injected signals and construct a reduced targeted bank. Finally, this targeted bank is used to identify potential lensed candidates for the targeted event from all possible data. For interested readers, please find the detailed description in [61].

As part of the LVK collaboration-wide paper to search for lensing signatures in the full third observation [38], the TESLA method was applied to all superthreshold events with a probability of astrophysical origin $p_{\text{astro}} > 0.5$ documented in [4] to search for their possible subthreshold lensed counterparts, should they exist. For each targeted search, we keep all candidates with a FAR < 1 in 30 days

TABLE I. Triggers for the target event GW191230_180458, whose median $\mathcal{M}_c^{\rm det}$ $[M_\odot] = 61.68$. The last three columns are the statistics calculated using the method proposed here (see Sec. II). LGW200104_184028 favors lensing through all three statistics. The rest of the triggers show no sufficient evidence of being lensed counterparts.

Subthreshold trigger	$\mathcal{M}_c^{\rm det}$ $[M_\odot]$	SNR	FAR $[\mathrm{yr}^{-1}]$	Δt [days]	$\mathcal{R}^{\rm gal}$	$\mathcal{B}^{\rm sky}$	$\mathcal{B}^{\rm masses}$
LGW200104_184028	58.20	8.48	6.59	5.02	4.43	1.77	0.91
LGW200301_075426	45.70	7.15	5.61	61.58	0.18	0.15	0.12
LGW200201_192756	20.50	7.80	5.11	33.06	0.57	0.02	0.00
LGW190818_232544	63.00	8.51	3.34	−133.78	0.02	0.03	0.99

(i.e., $<3.86 \times 10^{-7}$ Hz) and that pass a preliminary sky map overlap test [28] (See Ref. [38] for details).

For all the O3 events, altogether 472 possible subthreshold lensed candidates were found as a deeper internal candidate list,[3] of which only a small subset is reported in Table I [38]. Figure 4 shows the distribution of network SNRs of those superthreshold and subthreshold events. As expected, the subthreshold signals have lower SNRs as compared to superthreshold ones. Nevertheless, they all have SNR > 7. Moreover, 40% of the subthreshold events have SNR > 8. This is not necessarily surprising, given that in real noise, SNR is known to be suboptimal, relative to its performance in Gaussian noise. A more robust statistic, $p_{\rm astro}$ [63,64], is therefore used to segregate signals of astrophysical and terrestrial origin.

C. Rapid identification of the super-sub lensed candidates in O3

During the LVK full O3 lensing searches [38], only two out of all the above-mentioned targeted super-sub lensed pair candidates, pertaining to subthreshold events with the lowest FAR (i.e., the rate at which noise can falsely trigger a GW-like event) were followed up by a joint-parameter estimation analysis as implemented in the GOLUM pipeline [31]. None of those candidates showed any signatures of lensing. Here, we consider all the 472 search triggers and perform a preliminary analysis to rapidly identify the most interesting super-sub lensed candidates using the matched-filter estimates and the Bayestar sky maps. The chirp mass and sky maps overlap for the GW event pairs are captured in $\mathcal{B}^{\rm masses}$ and $\mathcal{B}^{\rm sky}$, respectively (see Sec. II).

In order to calculate the chirp mass overlap statistic $\mathcal{B}^{\rm masses}$, for the O3 super-sub pairs, we use the matched-filter estimates of $\mathcal{M}_c$ and ρ for the subthreshold triggers; whereas for the super-threshold events, we use the PE-based measurements from the open data available in GWOSC [52,65]. Note that PE and matched-filter chirp mass estimates can deviate significantly for a small fraction of events, as shown in Fig. 1.

Assuming a Gaussian distribution of the chirp mass likelihoods, using Eqs. (2) and (3), we calculate the

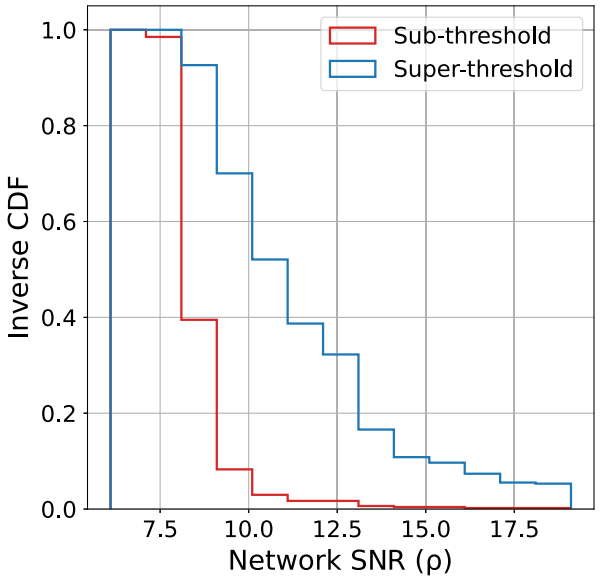

FIG. 4. Inverse cumulative distribution function of the network SNRs. The subthreshold triggers have lower SNRs as compared to superthreshold ones, but all of them have SNR > 7. In fact, 40% of the subthreshold events have SNR > 8.

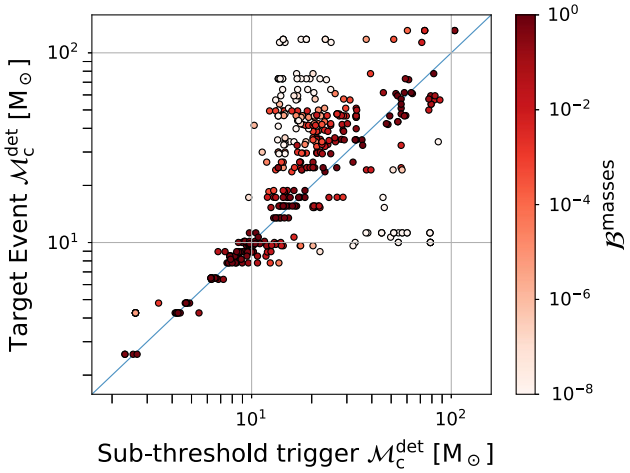

FIG. 5. Mean chirp mass estimates for the O3 super-sub candidate pairs and their $\mathcal{B}^{\rm masses}$. As expected, the majority of events with large $\mathcal{B}^{\rm masses}$ lie along the diagonal. The coefficient's value decreases for events situated away from the diagonal.

[3]The candidates having 90% credible region sky map overlap >0, taken from Table I of the data released in [62].

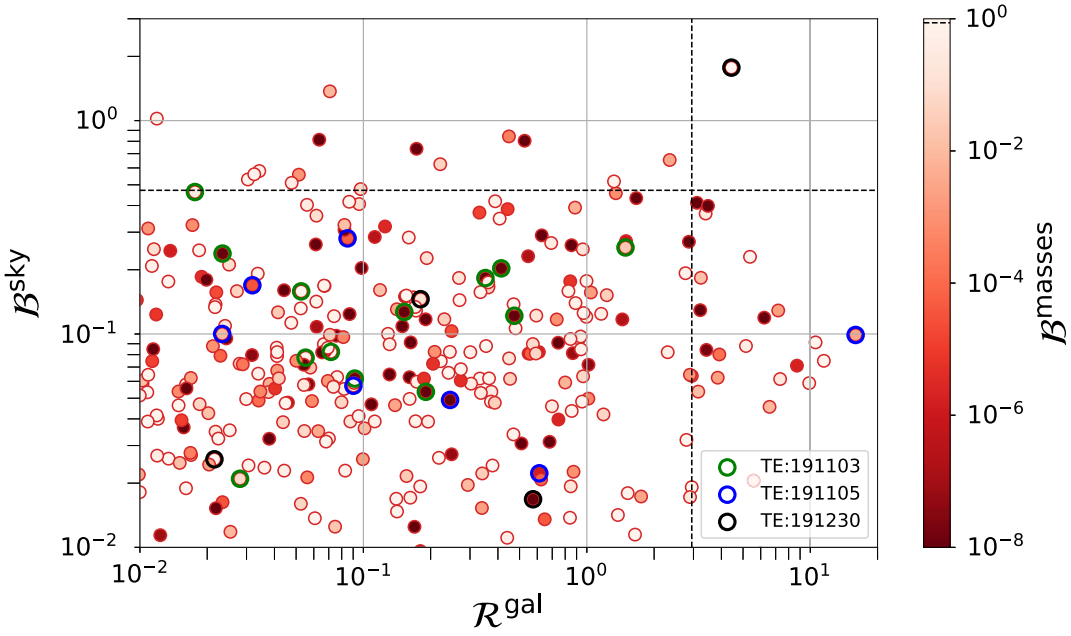

FIG. 6. Statistics for the individual super-sub pairs which were found by TESLA during the LVK full O3 lensing searches [38]. Black dashed lines represent the statistic value corresponding to the top-fifth percentile of all the pairs. An obvious, solitary outlier is identified in the top-right corner of the plot. In addition to being in the top-fifth percentile of the two statistics on the x and y axes, it is also in the top-fifth percentile of the statistic on the color bar (see the dashed black line there). We also highlight the triggers corresponding to the target events GW191103 (green), GW191105 (blue), and GW191230 (black).

Bhattacharyya coefficient $\mathcal{B}^{\rm masses}$ for each of the super-sub pairs. Figure 5 shows the mean estimates of chirp masses for the O3 super-sub pairs and their corresponding $\mathcal{B}^{\rm masses}$. As expected, the $\mathcal{B}^{\rm masses}$ is maximum along the diagonal—i.e., when the masses of the super-sub pair are similar. Note that $\mathcal{B}^{\rm masses}$ depends both on the mean and on the standard deviation of the two Gaussians; therefore, as we move away from the diagonal, it falls off, but not monotonically.

Next, we calculate the sky overlap statistic $\mathcal{B}^{\rm sky}$ [Eq. (5)], using the Bayestar sky maps of the subthreshold events and the more accurate PE sky maps of the superthreshold events. Finally, we estimate the $\mathcal{R}^{\rm gal}$ by using the trigger time information of the events. Figure 6 shows the time-delay statistic $\mathcal{R}^{\rm gal}$, the chirp-mass overlap $\mathcal{B}^{\rm masses}$, and the sky-overlap $\mathcal{B}^{\rm sky}$ statistics for each of the super-sub pairs. The dashed lines correspond to the top-fifth percentile statistic values of all the O3 pairs, which are found to be at $\mathcal{R}^{\rm gal} = 2.95$, $\mathcal{B}^{\rm sky} = 0.47$, and $\mathcal{B}^{\rm masses} = 0.87$, respectively. These are estimated from the distribution of the statistics for O3 super-sub pairs, as shown in Fig. 7. Since lensing is a rare event (rates of strong lensing vary from 0.01% to 0.1% [66,67]), we want to find the event pairs which are in the tails of the distribution of the three statistics as the lensing candidates. It should, however, be noted that the analysis could suffer from spurious biases (see Fig. 1), and hence should be followed up by a more comprehensive analysis.

The only pair which is in the top-fifth percentile of all three statistics is GW191230-LGW200104, with LGW200104 as the subthreshold counterpart to the superthreshold target event GW191230. Moreover, this pair has a time delay of only ∼5 days, which is more consistent with a lensed time delay than the temporal separation of two unrelated events drawn randomly from a Poisson process. The statistics values for this pair is $\mathcal{R}^{\rm gal} = 4.43$, $\mathcal{B}^{\rm sky} = 1.77$, and $\mathcal{B}^{\rm masses} = 0.9$. The good overlap of the sky maps for the pair is evident from Fig. 8. We conclude from our analysis that this pair is a (possibly lensed) outlier

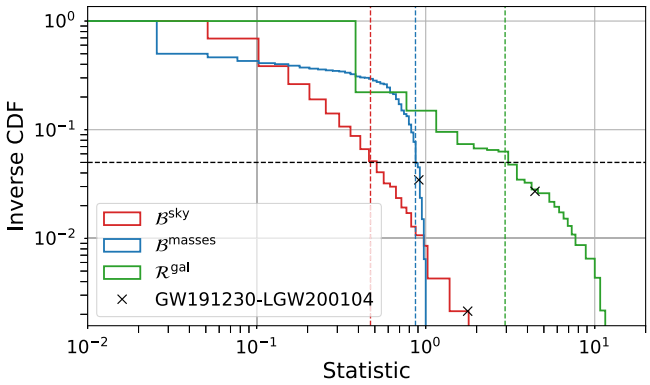

FIG. 7. Inverse cumulative distribution function of the statistics for the O3 super-sub pairs. The dashed lines correspond to the top-fifth percentile of the estimated values, which are found to be at $\mathcal{R}^{\rm gal} = 2.95$, $\mathcal{B}^{\rm sky} = 0.47$, and $\mathcal{B}^{\rm masses} = 0.87$, respectively. Only one event lies within this percentile across all three statistics, which is shown as a cross-mark (×).

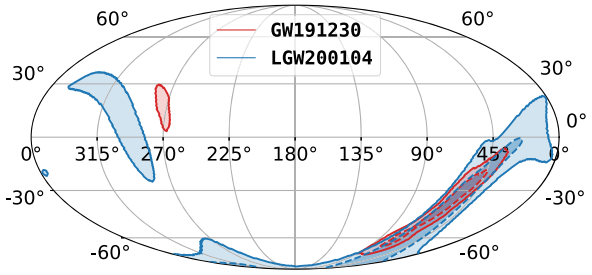

FIG. 8. Sky maps of GW191230 and LGW200104. The dark (light) shaded region represents the 50% (90%) contour. There is a significant visual overlap between the two sky maps. This is further corroborated by the high sky map overlap statistic value.

among the remaining population of (unlensed) O3 super-sub threshold pairs.

This pair was followed up by PE-based lensing analysis such as PO and joint-PE, in [49]. It turns out that after incorporating the lensing models and selection effects [32], this pair has the highest significance (i.e., the highest probability of being lensed) among all the O3 pairs, including the super-super threshold ones, with a caveat that LGW200104 might be of terrestrial origin, given that during the LVK online unlensed superthreshold searches, the event was found with the SPIIR [68,69] and CWB [70] pipelines, which reported a $p_{\rm astro}$ of 1% and a FAR of 4824.6/yr. This is in contrast to the FAR of 6.59/yr estimated by TESLA. We report these numbers for the benefit of the reader, and do not attempt to draw any conclusions about the nature (noise or signal) of LGW200104. Our method gives a *preliminary* assessment of whether LGW200104 is a lensed counterpart to GW191230, *assuming* the former is a signal, which it may well *not* be. We follow the LVK naming convention of the GW candidates—i.e., *GWYYMMDD_hhmmss*—encoding the date and coordinated Universal Time

TABLE II. Triggers for the target event GW191105_143521, whose median $\mathcal{M}_c^{\rm det}\ [M_\odot] = 9.62$. The last three columns are the statistics calculated using the method proposed (see Sec. II). LGW191106_200820 has a significant time-delay statistic ($\mathcal{R}^{\rm gal}$), but it is ruled out by the remaining two. The rest of the triggers show no signatures of being lensed counterparts.

Subthreshold trigger	$\mathcal{M}_c^{\rm det}\ [M_\odot]$	SNR	FAR $[{\rm yr}^{-1}]$	Δt [days]	$\mathcal{R}^{\rm gal}$	$\mathcal{B}^{\rm sky}$	$\mathcal{B}^{\rm masses}$
LGW191106_200820	14.40	8.36	0.53	1.23	15.95	0.10	0.00
LGW200128_115458	17.60	7.80	7.57	83.89	0.08	0.28	0.00
LGW191207_050023	20.30	7.87	3.04	31.60	0.61	0.02	0.00
LGW191229_024823	32.20	9.08	12.05	53.51	0.24	0.05	0.00
LGW200303_074125	17.50	8.13	5.87	118.71	0.03	0.17	0.00
LGW200126_135203	11.90	7.72	6.75	81.97	0.09	0.06	0.17
LGW200315_070710	14.10	7.70	10.91	130.69	0.02	0.10	0.01

TABLE III. Triggers for the target event GW191103_012549, whose median $\mathcal{M}_c^{\rm det}\ [M_\odot] = 10.01$. The last three columns are the statistics calculated using the proposed method (see Sec. II). None of the candidates shows signatures of being lensed.

Subthreshold trigger	$\mathcal{M}_c^{\rm det}\ [M_\odot]$	SNR	FAR $[{\rm yr}^{-1}]$	Δt [days]	$\mathcal{R}^{\rm gal}$	$\mathcal{B}^{\rm sky}$	$\mathcal{B}^{\rm masses}$
LGW191118_113217	14.00	8.08	6.02	15.42	1.49	0.25	0.02
LGW191213_164018	78.60	10.40	0.32	40.64	0.41	0.20	0.00
LGW190919_131654	33.00	9.15	2.89	−44.51	0.35	0.18	0.00
LGW190926_133040	78.60	7.10	7.57	−37.50	0.47	0.12	0.00
LGW190828_192315	54.30	7.37	6.24	−66.25	0.15	0.13	0.00
LGW200102_033257	78.60	7.18	0.57	60.09	0.19	0.05	0.00
LGW200211_024259	9.44	8.11	5.87	100.05	0.05	0.16	0.81
LGW200323_135352	8.59	8.25	9.02	141.52	0.02	0.46	0.33
LGW190805_134348	10.40	8.79	0.29	−89.49	0.07	0.08	0.87
LGW190813_125024	78.60	7.14	5.61	−81.52	0.09	0.06	0.00
LGW200312_144311	78.60	7.29	8.14	130.55	0.02	0.24	0.00
LGW190727_144658	8.97	8.39	2.76	−98.44	0.06	0.08	0.55
LGW190517_114359	78.60	7.40	0.85	−169.57	0.01	0.28	0.00
LGW190401_190150	54.30	8.31	5.68	−215.27	0.00	0.36	0.00
LGW200305_153119	13.00	8.61	4.92	123.59	0.03	0.02	0.06

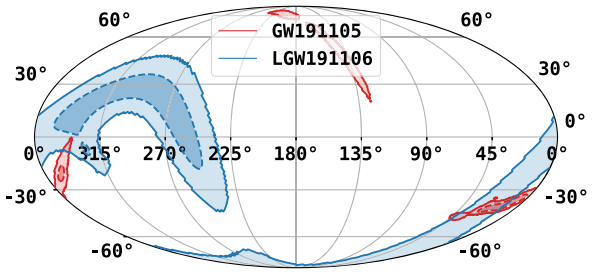

FIG. 9. Sky maps of GW191105 and LGW191106. The dark (light) shaded region represents the 50% (90%) contour. The sky map overlap is even visually seen to be modest and is also evidenced in the low sky map overlap statistic value.

(UTC) of the signal [4]. Table I shows the rest of the triggers found in the searches with the target event GW191230. All of them have at least one of the statistics whose value is low enough to be relegated as unworthy of follow-up.

Special target events: GW191103_012549 and GW191105_143521. During the LVK full O3 strong lensing searches [38], events pair GW191103_012549–GW191105_143521, which we call GW191103-GW191105 from now on, was found to be among the more significant ($\sim 1\sigma$) pairs, though unlikely to be lensed. The pair is also analyzed in detail in [49], finding no conclusive evidence for lensing. Typically, galaxy lenses can produce more than two images of a GW source. Any additional subthreshold lensed counterpart to the pair GW191103-GW191105, if found, can help us in increasing its significance of being lensed, in the reconstruction of lens configuration and in localizing the source to a host galaxy through cross-matching of electromagnetically observed lensed galaxy catalogues [37,71]. In the O3 data, 15 potential counterparts for GW191103 and 7 for GW191105 were found by the TESLA method (see Sec. III B), but none of them is in common for both the targeted events. The rapid statistics for each of them are shown in Tables II and III. LGW191106_200820 was also considered to be a potentially lensed counterpart of GW191105, by virtue of having the highest $\mathcal{R}^{\rm gal} = 15.95$. However, the poor sky map overlap ($\mathcal{B}^{\rm sky} = 0.1$) and even poorer Bhattacharya coefficient value resulted in this event being relegated as unworthy of follow-up. The sky maps for this pair are shown in Fig. 9. In summary, we conclude that *no* obvious strongly lensed subthreshold counterpart to the GW191103-GW191105 pair is found with our preliminary analysis.

IV. SUMMARY AND OUTLOOK

A large number of targeted subthreshold events opens the possibility of one or more of them being lensed (demagnified) counterparts of confidently detected superthreshold events. Identifying such subthreshold lensed counterparts using conventional methods involving large-scale parameter estimation exercises overburdens computational resources. Thus, a preliminary method that rapidly weeds out "obviously" unlensed super-sub candidate pairs is required. In this work, we have proposed one possible rapid and computationally inexpensive identification scheme. The method is conceptually similar to the PO statistic while relying on approximations to posteriors on chirp masses and sky location pertaining to the subthreshold counterpart.

A Bhattacharyya coefficient, $\mathcal{B}^{\rm masses}$, is constructed from the approximations of the chirp mass likelihood. A sky map overlap statistic, $\mathcal{B}^{\rm sky}$, is constructed from Bayestar sky maps of subthreshold events and PE sky maps of superthreshold events. The method additionally uses prior information on expected lensed time delays, assuming a lens profile and a SDSS-catalog-fitted model for lens parameter distributions, to further enhance its discriminating abilities. Accordingly, an $\mathcal{R}^{\rm gal}$ statistic is constructed.

Using this method, the vast majority of subthreshold events were found to be unrelated to the superthreshold events that were targeted. However, one interesting super-sub candidate pair was found to be an outlier—its $\mathcal{B}^{\rm masses,sky}$, and $\mathcal{R}^{\rm gal}$ statistic values were *all* found to be within the highest-fifth percentile of the super-sub candidate pair values analyzed. The follow-up analysis of the pair in [49] by more sophisticated joint-PE analyses, that also include selection effects [32], deemed this event to be among the more significant lensed candidates among all analyzed candidate pairs—super-super and super-sub, assuming a singular isothermal ellipsoid lens profile. While the significance of the event was still not sufficient to claim the detection of a lensed pair, in part because LGW200104 had a very low $p_{\rm astro}$, the identification of this event using our method motivates the need for rapid and computationally inexpensive analyses for future observing runs, where the number of candidate pairs is expected to grow drastically.

In future work, we intend to further assess the performance of our method in more realistic simulated datasets. In particular, we plan to inject subthreshold lensed and unlensed events, in addition to superthreshold events, in real noise. We then plan to perform a matched-filter search for these events to acquire matched-filter parameter values of chirp masses and arrival times. Using these, and the Bayestar sky maps, we plan to reconstruct the ROCs to assess the performance in comparison to the PO statistic, to check if the loss in efficiency relative to PO is still acceptable.

Typically, a PE run of a BBH event takes $\mathcal{O}$(days) and $\mathcal{O}$(weeks) for joint-PE lensing analysis, whereas the methodology developed here takes $\mathcal{O}$(minutes) to reconstruct the posteriors and evaluate the three statistics. In future observing runs, the number of events is expected to grow exponentially; therefore, our approximate method

could be very useful. We additionally plan to explore the possibility of using PE products from PE algorithms that can rapidly generate posterior samples, such as heterodyning methods [72–74] and machine-learning-based [29,75,76] methods, among others [77]. These products will likely be a nontrivial improvement over those that were used in the method presented in this work, although this conjecture needs to be tested, especially for subthreshold events.

ACKNOWLEDGMENTS

We are thankful to P. Ajith, D. Chatterjee, H. Fong, and A. Barsode along with the astrophysical relativity group at ICTS and the LVK lensing group for helpful discussions and suggestions. We are also thankful to D. Keitel, M. Wright, and J. Janquart for their careful reading of this manuscript. Juno C. L. Chan acknowledges support from the Villum Investigator program supported by VILLUM FONDEN (Grant No. 37766) and the DNRF Chair, by the Danish Research Foundation. J. R. Cudell benefits from the support of the Fonds de la Recherche Scientifique-FNRS, Belgium, under Grant No. 4.4501.19. The authors are grateful for computational resources provided by the LIGO Laboratory and supported by National Science Foundation Grants No. PHY-0757058 and No. PHY-0823459. This research has made use of data or software obtained from the Gravitational Wave Open Science Center, a service of LIGO Laboratory, the LIGO Scientific Collaboration, the Virgo Collaboration, and KAGRA. LIGO Laboratory and Advanced LIGO are funded by the United States National Science Foundation (NSF), as well as the Science and Technology Facilities Council (STFC) of the United Kingdom, the Max-Planck-Society (MPS), and the State of Niedersachsen/Germany for support of the construction of Advanced LIGO and construction and operation of the GEO600 detector. Additional support for Advanced LIGO was provided by the Australian Research Council. Virgo is funded, through the European Gravitational Observatory (EGO), by the French Centre National de Recherche Scientifique (CNRS), the Italian Istituto Nazionale di Fisica Nucleare (INFN), and the Dutch Nikhef, with contributions by institutions from Belgium, Germany, Greece, Hungary, Ireland, Japan, Monaco, Poland, Portugal, and Spain. K.A.G.R.A. is supported by the Ministry of Education, Culture, Sports, Science and Technology (MEXT), the Japan Society for the Promotion of Science (JSPS) in Japan; the National Research Foundation (NRF) and Ministry of Science and ICT (MSIT) in Korea; the Academia Sinica (AS) and National Science and Technology Council (NSTC) in Taiwan. This material is based upon work supported by NSF's LIGO Laboratory, which is a major facility fully funded by the National Science Foundation. A. K. Y. L. would like to gratefully acknowledge the support from the National Science Foundation through the Grants NSF PHY-1912594 and NSF PHY-2207758.

[1] J Aasi *et al.*, Advanced LIGO, Classical Quantum Gravity **32**, 074001 (2015).
[2] F Acernese *et al.*, Advanced Virgo: A second-generation interferometric gravitational wave detector, Classical Quantum Gravity **32**, 024001 (2015).
[3] Yoichi Aso, Yuta Michimura, Kentaro Somiya, Masaki Ando, Osamu Miyakawa, Takanori Sekiguchi, Daisuke Tatsumi, and Hiroaki Yamamoto (KAGRA Collaboration), Interferometer design of the KAGRA gravitational wave detector, Phys. Rev. D **88**, 043007 (2013).
[4] R. Abbott *et al.* (LIGO Scientific, Virgo, and KAGRA Collaborations), GWTC-3: Compact binary coalescences observed by LIGO and Virgo during the second part of the third observing run, Phys. Rev. X **13**, 041039 (2023).
[5] Barak Zackay, Liang Dai, Tejaswi Venumadhav, Javier Roulet, and Matias Zaldarriaga, Detecting gravitational waves with disparate detector responses: Two new binary black hole mergers, Phys. Rev. D **104**, 063030 (2021).
[6] Tejaswi Venumadhav, Barak Zackay, Javier Roulet, Liang Dai, and Matias Zaldarriaga, New binary black hole mergers in the second observing run of Advanced LIGO and Advanced Virgo, Phys. Rev. D **101**, 083030 (2020).
[7] Barak Zackay, Tejaswi Venumadhav, Liang Dai, Javier Roulet, and Matias Zaldarriaga, Highly spinning and aligned binary black hole merger in the Advanced LIGO first observing run, Phys. Rev. D **100**, 023007 (2019).
[8] Seth Olsen, Tejaswi Venumadhav, Jonathan Mushkin, Javier Roulet, Barak Zackay, and Matias Zaldarriaga, New binary black hole mergers in the LIGO-Virgo O3a data, Phys. Rev. D **106**, 043009 (2022).
[9] Alexander H. Nitz, Sumit Kumar, Yi-Fan Wang, Shilpa Kastha, Shichao Wu, Marlin Schäfer, Rahul Dhurkunde, and Collin D. Capano, 4-OGC: Catalog of gravitational waves from compact-binary mergers, arXiv:2112.06878.
[10] Benjamin P. Abbott *et al.* (Virgo and LIGO Scientific Collaborations), GW170817: Observation of gravitational waves from a binary neutron star inspiral, Phys. Rev. Lett. **119**, 161101 (2017).
[11] B. P. Abbott *et al.* (LIGO Scientific and Virgo Collaborations), GW190425: Observation of a compact binary coalescence with total mass $\sim 3.4 M_{\odot}$, Astrophys. J. Lett. **892**, L3 (2020).
[12] B. P. Abbott *et al.* (LIGO Scientific and Virgo Collaborations), Observation of gravitational waves from two neutron

star-black hole coalescences, Astrophys. J. Lett. **915**, L5 (2021).
[13] R. Abbott, T. D. Abbott, F. Acernese, K. Ackley, C. Adams, N. Adhikari, R. X. Adhikari, V. B. Adya, C. Affeldt, D. Agarwal *et al.* (LIGO Scientific, Virgo, and KAGRA Collaborations), The population of merging compact binaries inferred using gravitational waves through GWTC-3, Phys. Rev. X **13**, 011048 (2023).
[14] B. P. Abbott *et al.* (LIGO Scientific, Virgo, and KAGRA Collaborations), A gravitational-wave standard siren measurement of the Hubble constant, Nature (London) **551**, 85 (2017).
[15] R. Abbott, H. Abe, F. Acernese, K. Ackley, N. Adhikari, R. X. Adhikari, V. K. Adkins, V. B. Adya, C. Affeldt, D. Agarwal *et al.* (LIGO Scientific, Virgo, and KAGRA Collaborations), Tests of general relativity with GWTC-3, arXiv:2112.06861.
[16] B. P. Abbott *et al.* (LIGO Scientific and Virgo Collaborations), GW170817: Measurements of neutron star radii and equation of state, Phys. Rev. Lett. **121**, 161101 (2018).
[17] Hans C. Ohanian, On the focusing of gravitational radiation, Int. J. Theor. Phys. **9**, 425 (1974).
[18] S. Deguchi and W. D. Watson, Diffraction in gravitational lensing for compact objects of low mass, Astrophys. J. **307**, 30 (1986).
[19] Yun Wang, Albert Stebbins, and Edwin L. Turner, Gravitational lensing of gravitational waves from merging neutron star binaries, Phys. Rev. Lett. **77**, 2875 (1996).
[20] Takahiro T. Nakamura, Gravitational lensing of gravitational waves from inspiraling binaries by a point mass lens, Phys. Rev. Lett. **80**, 1138 (1998).
[21] Ken K. Y. Ng, Kaze W. K. Wong, Tom Broadhurst, and Tjonnie G. F. Li, Precise LIGO lensing rate predictions for binary black holes, Phys. Rev. D **97**, 023012 (2018).
[22] Liang Dai, Tejaswi Venumadhav, and Kris Sigurdson, Effect of lensing magnification on the apparent distribution of black hole mergers, Phys. Rev. D **95**, 044011 (2017).
[23] Graham P Smith, Mathilde Jauzac, John Veitch, Will M Farr, Richard Massey, and Johan Richard, What if LIGO's gravitational wave detections are strongly lensed by massive galaxy clusters?, Mon. Not. R. Astron. Soc. **475**, 3823 (2018).
[24] Shun-Sheng Li, Shude Mao, Yuetong Zhao, and Youjun Lu, Gravitational lensing of gravitational waves: A statistical perspective, Mon. Not. R. Astron. Soc. **476**, 2220 (2018).
[25] K. Haris, Ajit Kumar Mehta, Sumit Kumar, Tejaswi Venumadhav, and Parameswaran Ajith, Identifying strongly lensed gravitational wave signals from binary black hole mergers, arXiv:1807.07062.
[26] Liang Dai and Tejaswi Venumadhav, On the waveforms of gravitationally lensed gravitational waves, arXiv:1702.04724.
[27] Jose María Ezquiaga, Daniel E. Holz, Wayne Hu, Macarena Lagos, and Robert M. Wald, Phase effects from strong gravitational lensing of gravitational waves, Phys. Rev. D **103**, 064047 (2021).
[28] Henry W. Y. Wong, Lok W. L. Chan, Isaac C. F. Wong, Rico K. L. Lo, and Tjonnie G. F. Li, Using overlap of sky localization probability maps for filtering potentially lensed pairs of gravitational-wave signals, arXiv:2112.05932.
[29] Srashti Goyal, D. Harikrishnan, Shasvath J. Kapadia, and Parameswaran Ajith, Rapid identification of strongly lensed gravitational-wave events with machine learning, Phys. Rev. D **104**, 124057 (2021).
[30] Xiaoshu Liu, Ignacio Magana Hernandez, and Jolien Creighton, Identifying strong gravitational-wave lensing during the second observing run of Advanced LIGO and Advanced Virgo, Astrophys. J. **908**, 97 (2021).
[31] Justin Janquart, Otto A. Hannuksela, K. Haris, and Chris Van Den Broeck, Golum: A fast and precise methodology to search for, and analyze, strongly lensed gravitational-wave events, arXiv:2203.06444.
[32] Rico K. L. Lo and Ignacio Magana Hernandez, A Bayesian statistical framework for identifying strongly-lensed gravitational-wave signals, Phys. Rev. D **107**, 123015 (2023).
[33] Connor McIsaac, David Keitel, Thomas Collett, Ian Harry, Simone Mozzon, Oliver Edy, and David Bacon, Search for strongly lensed counterpart images of binary black hole mergers in the first two LIGO observing runs, Phys. Rev. D **102**, 084031 (2020).
[34] B. P. Abbott *et al.* (LIGO Scientific, Virgo, and KAGRA Collaborations), GWTC-1: A gravitational-wave transient catalog of compact binary mergers observed by LIGO and Virgo during the first and second observing runs, Phys. Rev. X **9**, 031040 (2019).
[35] R. Abbott *et al.* (LIGO Scientific, Virgo, and KAGRA Collaborations), GWTC-2: Compact binary coalescences observed by LIGO and Virgo during the first half of the third observing run, Phys. Rev. X **11**, 021053 (2021).
[36] R. Abbott *et al.* (LIGO Scientific and Virgo Collaborations), Search for lensing signatures in the gravitational-wave observations from the first half of LIGO-Virgo's third observing run, Astrophys. J. **923**, 14 (2021).
[37] O. A. Hannuksela, K. Haris, K. K. Y. Ng, S. Kumar, A. K. Mehta, D. Keitel, T. G. F. Li, and P. Ajith, Search for gravitational lensing signatures in LIGO-Virgo binary black hole events, Astrophys. J. Lett. **874**, L2 (2019).
[38] The LIGO Scientific, the Virgo, and the KAGRA Collaborations, Search for gravitational-lensing signatures in the full third observing run of the LIGO-Virgo network, arXiv:2304.08393.
[39] A. Renske A. C. Wierda, Ewoud Wempe, Otto A. Hannuksela, Léon V. E. Koopmans, and Chris Van Den Broeck, Beyond the detector horizon: Forecasting gravitational-wave strong lensing, Astrophys. J. **921**, 154 (2021).
[40] Alvin K. Y. Li, Rico K. L. Lo, Surabhi Sachdev, C. L. Chan, E. T. Lin, Tjonnie G. F. Li, and Alan J. Weinstein, Targeted sub-threshold search for strongly-lensed gravitational-wave events, arXiv:1904.06020.
[41] Connor McIsaac, David Keitel, Thomas Collett, Ian Harry, Simone Mozzon, Oliver Edy, and David Bacon, Search for strongly lensed counterpart images of binary black hole mergers in the first two LIGO observing runs, Phys. Rev. D **102**, 084031 (2020).
[42] Liang Dai, Barak Zackay, Tejaswi Venumadhav, Javier Roulet, and Matias Zaldarriaga, Search for lensed gravitational waves including morse phase information: An intriguing candidate in O2, arXiv:2007.12709.
[43] R. Abbott *et al.* (The LIGO Scientific and the Virgo Collaborations), GWTC-2.1: Deep extended catalog of

compact binary coalescences observed by LIGO and Virgo during the first half of the third observing run, Phys. Rev. D **109**, 022001 (2024).
[44] LIGO Scientific and Virgo Collaborations, GWTC-2.1: Deep extended catalog of compact binary coalescences observed by LIGO and Virgo during the first half of the third observing run—parameter estimation data release (2022), 10.5281/zenodo.5546662.
[45] LIGO Scientific, Virgo, and KAGRA Collaborations, GWTC-3: Compact binary coalescences observed by LIGO and Virgo during the second part of the third observing run—parameter estimation data release (2021).
[46] Curt Cutler and Éanna E. Flanagan, Gravitational waves from merging compact binaries: How accurately can one extract the binary's parameters from the inspiral waveform? Phys. Rev. D **49**, 2658 (1994).
[47] A. Bhattacharyya, On a measure of divergence between two multinomial populations, Sankhyā **7**, 401 (1946).
[48] Leo P. Singer and Larry R. Price, Rapid Bayesian position reconstruction for gravitational-wave transients, Phys. Rev. D **93**, 024013 (2016).
[49] Justin Janquart *et al.*, Follow-up analyses to the O3 LIGO-Virgo-KAGRA lensing searches, Mon. Not. R. Astron. Soc. **526**, 3 (2023).
[50] Anupreeta More and Surhud More, Improved statistic to identify strongly lensed gravitational wave events, Mon. Not. R. Astron. Soc. **515**, 1044 (2022).
[51] Mesut Çalışkan, Jose María Ezquiaga, Otto A. Hannuksela, and Daniel E. Holz, Lensing or luck? False alarm probabilities for gravitational lensing of gravitational waves, Phys. Rev. D **107**, 063023 (2023).
[52] The LIGO Scientific, the Virgo, and the KAGRA Collaborations, Open data from the third observing run of LIGO, Virgo, KAGRA and GEO, Astrophys. J. Suppl. Ser. **267**, 29 (2023).
[53] Alex Nitz *et al.*, gwastro/pycbc: Pycbc release 1.16.4 (2020), 10.5281/zenodo.3904502.
[54] Kipp Cannon *et al.*, GstLAL: A software framework for gravitational wave discovery, arXiv:2010.05082.
[55] Samantha A. Usman *et al.*, The PyCBC search for gravitational waves from compact binary coalescence, Classical Quantum Gravity **33**, 215004 (2016).
[56] Masamune Oguri, Effect of gravitational lensing on the distribution of gravitational waves from distant binary black hole mergers, Mon. Not. R. Astron. Soc. **480**, 3842 (2018).
[57] Yun-Young Choi, Changbom Park, and Michael S. Vogeley, Internal and collective properties of galaxies in the Sloan Digital Sky Survey, Astrophys. J. **658**, 884 (2007).
[58] The Virgo Collaboration, Advanced Virgo sensitivity curve study, Technical Report No. VIR-0073D-12, Virgo Collaboration, 2012.
[59] The updated Advanced LIGO design curve, Technical Report No. LIGO-T1800044-v5, LIGO Document Control Center, 2018.
[60] Alex Nitz *et al.*, gwastro/pycbc: Pycbc release v1.16.8 (2020), 10.5281/zenodo.3985815.
[61] Alvin K. Y. Li, Rico K. L. Lo, Surabhi Sachdev, C. L. Chan, E. T. Lin, Tjonnie G. F. Li, and Alan J. Weinstein, Targeted sub-threshold search for strongly-lensed gravitational-wave events, Phys. Rev. D **107**, 123014 (2023).
[62] LIGO Scientific, Virgo, and KAGRA Collaborations, Search for gravitational-lensing signatures in the full third observing run of the LIGO-Virgo network, arXiv:2304.08393.
[63] Will M. Farr, Jonathan R. Gair, Ilya Mandel, and Curt Cutler, Counting and confusion: Bayesian rate estimation with multiple populations, Phys. Rev. D **91**, 023005 (2015).
[64] Shasvath J. Kapadia *et al.*, A self-consistent method to estimate the rate of compact binary coalescences with a Poisson mixture model, Classical Quantum Gravity **37**, 045007 (2020).
[65] R. Abbott *et al.*, Open data from the first and second observing runs of Advanced LIGO and Advanced Virgo, SoftwareX **13**, 100658 (2021).
[66] Fei Xu, Jose Maria Ezquiaga, and Daniel E. Holz, Please repeat: Strong lensing of gravitational waves as a probe of compact binary and galaxy populations, Astrophys. J. **929**, 9 (2022).
[67] A. Renske A. C. Wierda, Ewoud Wempe, Otto A. Hannuksela, Lé on V. E. Koopmans, and Chris Van Den Broeck, Beyond the detector horizon: Forecasting gravitational-wave strong lensing, Astrophys. J. **921**, 154 (2021).
[68] Jing Luan, Shaun Hooper, Linqing Wen, and Yanbei Chen, Towards low-latency real-time detection of gravitational waves from compact binary coalescences in the era of advanced detectors, Phys. Rev. D **85**, 102002 (2012).
[69] Qi Chu *et al.*, SPIIR online coherent pipeline to search for gravitational waves from compact binary coalescences, Phys. Rev. D **105**, 024023 (2022).
[70] S. Klimenko *et al.*, Method for detection and reconstruction of gravitational wave transients with networks of advanced detectors, Phys. Rev. D **93**, 042004 (2016).
[71] Ewoud Wempe, Léon V. E. Koopmans, A. Renske A. C. Wierda, Otto Akseli Hannuksela, and Chris van den Broeck, A lensing multi-messenger channel: Combining LIGO-Virgo-KAGRA lensed gravitational-wave measurements with Euclid observations, arXiv:2204.08732.
[72] Tousif Islam, Javier Roulet, and Tejaswi Venumadhav, Factorized parameter estimation for real-time gravitational wave inference, arXiv:2210.16278.
[73] Javier Roulet, Seth Olsen, Jonathan Mushkin, Tousif Islam, Tejaswi Venumadhav, Barak Zackay, and Matias Zaldarriaga, Removing degeneracy and multimodality in gravitational wave source parameters, Phys. Rev. D **106**, 123015 (2022).
[74] Neil J. Cornish, Rapid and robust parameter inference for binary mergers, Phys. Rev. D **103**, 104057 (2021).
[75] Maximilian Dax, Stephen R. Green, Jonathan Gair, Jakob H. Macke, Alessandra Buonanno, and Bernhard Schölkopf, Real-time gravitational wave science with neural posterior estimation, Phys. Rev. Lett. **127**, 241103 (2021).
[76] Hunter Gabbard, Chris Messenger, Ik Siong Heng, Francesco Tonolini, and Roderick Murray-Smith, Bayesian parameter estimation using conditional variational autoencoders for gravitational-wave astronomy, Nat. Phys. **18**, 112 (2021).
[77] Lalit Pathak, Amit Reza, and Anand S. Sengupta, Rapid reconstruction of compact binary sources using meshfree approximation, Phys. Rev. D **108**, 064055 (2023).
[78] gwosc.org.